Available online at www.sciencedirect.com
ScienceDirect
Geochimica et Cosmochimica Acta xxx (2008) xxx–xxx
Geochimica et Cosmochimica Acta
www.elsevier.com/locate/gca

Experimental determination of growth rate effect on U^{6+} and Mg^{2+} partitioning between aragonite and fluid at elevated U^{6+} concentration

R.I. Gabitov [a,b,*], G.A. Gaetani [b], E.B. Watson [a], A.L. Cohen [b], H.L. Ehrlich [a]

[a] Department of Earth and Environmental Sciences, Rensselaer Polytechnic Institute, Troy, NY 12180, USA
[b] Department of Geology and Geophysics, Woods Hole Oceanographic Institution, Woods Hole, MA 02543, USA

Received 30 August 2007; accepted in revised form 21 May 2008

Abstract

Results are reported from an experimental study in which the partitioning of U and Mg between aragonite and an aqueous solution were determined as a function of crystal growth rate. Crystals, identified as aragonite by X-ray diffractometry and micro-Raman spectroscopy, were grown by diffusion of CO_2 from an ammonium carbonate source into a calcium-bearing solution at temperatures of 22 and 53 °C. Hemispherical bundles (spherulites) of aragonite crystals were produced, the growth rates of which decreased monotonically from the spherulite interiors to the edges and thus provide the opportunity to examine the influence of growth rate on crystal composition. Element concentration ratios were measured using electron microprobe (EMP) and fluid composition was determined by inductively coupled plasma-mass spectrometry (ICP-MS) and atomic absorption (AA). Growth rates were determined directly by addition of a Dy spike to the fluid during the experiment that was subsequently located in an experimentally precipitated spherulite using secondary ion mass spectrometry (SIMS). At 22 °C both U/Ca and Mg/Ca partition coefficients exhibited a strong growth rate dependence when crystal growth rates were low, and became independent of growth rate when crystal growth rates were high. The U/Ca ratios in aragonite increase between 22 and 53 °C; in contrast Mg/Ca ratios show inverse dependence on temperature.

1. INTRODUCTION

Aragonite is a polymorph of calcium carbonate ($CaCO_3$) is used by many marine invertebrates including corals, many mollusks, sclerosponges and pteropods to build hard skeletons. Because the chemical composition of aragonite varies with changes in seawater temperature and chemistry, such skeletons preserved in the geologic record have the potential to provide quantitative information about seawater temperatures and chemical compositions through time. The uranium-to-calcium (U/Ca) and magnesium-to-calcium (Mg/Ca) ratios of coral skeleton have been explored as potential paleothermometers (Wei et al., 2000; Cardinal et al., 2001; Watanabe et al., 2001; Quinn and Sampson, 2002). In general, the Mg/Ca ratios in corals increase with increasing temperature while U/Ca ratios show an inverse correlation with temperature (Shen and Dunbar, 1994; Min et al., 1995; Mitsuguchi et al., 1996; Sinclair et al., 1998; Reynaud et al., 2007). Nevertheless, inconsistencies in the relationship between temperature and compositional variability amongst different corals and amongst different aragonite-accreting taxa that have experienced the same seawater conditions suggest that factors other than temperature influence the Mg/Ca and U/Ca ratios of coral and other biogenic aragonites. Additional evidence for the influence of factors other than temperature on skeletal Mg/Ca and U/Ca ratios comes from analyses of coral skeletons at nano- and micron-scale resolution. Over these length scales – which represent time scales over which

* Corresponding author. Address: Division of Geological and Planetary Sciences, California Institute of Technology, Pasadena, CA 91125, USA.
E-mail address: gabitr@gps.caltech.edu (R.I. Gabitov).

0016-7037/$ - see front matter © 2008 Elsevier Ltd. All rights reserved.
doi:10.1016/j.gca.2008.05.047

temperatures are relatively invariant – both Mg/Ca and U/Ca ratios exhibit large-amplitude oscillations more-or-less coincident with variations in skeletal microstructure (Meibom et al., 2004, 2006; Robinson et al., 2006; Sinclair et al., 2006; Gagnon et al., 2007).

It is well established that crystal growth rate influences the element-to-calcium ratio in calcite (Lorens, 1981; Tesoriero and Pankow, 1996; Gabitov and Watson, 2006). However, little information is yet available on growth rate effects on element:calcium ratios in aragonite. In this study, we investigated the effects of crystal growth rate on the partitioning of U and Mg between aragonite and aqueous fluid at two different temperatures. In previous experimental studies involving aragonite, partition coefficients ($K_d^i = X_i^{\text{Aragonite}} X_{\text{Ca}}^{\text{Fluid}} / X_{\text{Ca}}^{\text{Aragonite}} X_i^{\text{Fluid}}$, where i is the cation of interest and X is the mole fraction) were calculated from analyses of bulk samples of crystals precipitated in the experiments (see Kitano and Oomori, 1971; Zhong and Mucci, 1989; Meece and Benninger, 1993). Bulk precipitation rates reflect a combination of crystal nucleation and growth rates. Mechanisms capable of producing growth rate-dependent partitioning are sensitive to the velocity at which the mineral-fluid interface advances during crystal growth (i.e., linear growth rate). Therefore, bulk precipitation data cannot be used directly to understand growth rate-dependent partitioning of U/Ca and Mg/Ca between aragonite and fluid. Further, multiple carbonates are often present in the bulk precipitate at temperatures below ~35 °C (Kinsman and Holland, 1969). Even 1% calcite (the typical detection limit of X-ray diffraction) in the bulk precipitate may significantly affect the Mg/Ca ratio of the bulk $CaCO_3$. This presents an additional challenge in the interpretation of element partitioning data for carbonates precipitated at low temperatures.

In this study, we investigated effects of growth rate and temperature on Mg and U incorporation into aragonite using a microbeam analytical technique (EMP or SIMS). The ratios of Mg/Ca and U/Ca were measured within single, hemispherical bundles of aragonite crystals at discrete, successive spots along their growth axes, tracking the change in elemental composition as growth rate slowed from the core to the edge of each bundle. Experiments were conducted at 22 and 53 °C and growth rates (V) were determined in the 22 °C experiment. The resulting values of V ranged from 0.044 to 30 nm/s, or 3.5 to 2592 μm/day. Estimates of extension rates of aragonite crystals fibers within fiber bundles that make up the bulk of coral skeletons, range from ~2 to 30 μm per day i.e., at the low end of our experimental range (Cohen et al., 2001; Cohen and Thorrold, 2007).

2. EXPERIMENTAL AND ANALYTICAL TECHNIQUES

Two experiments were conducted in which aragonite crystals were precipitated from an aqueous chloride solution at 22 and 53 °C using the method described by Gruzensky (1967). Carbon dioxide from decomposing ammonium carbonate diffused into the chloride solution increasing the concentration of CO_3^{2-} and leading to precipitation of aragonite. Experiment D-1 was carried out at 22 °C using a solution containing 0.5 mol/l NH_4Cl, 0.05 mol/l $MgCl_2$, 0.01 mol/l $CaCl_2$ and 2.88×10^{-5} mol/l $UO_2(NO_3)_2$. Experiment D-2 was conducted at 53 °C using a solution containing 0.5 mol/l NaCl, 0.05 mol/l $MgCl_2$, 0.01 mol/l $CaCl_2$, 2.88×10^{-5} mol/l $UO_2(NO_3)_2$ solutions. Both solutions had ionic strengths close to that of seawater (0.69). A calcite powder (99.9965%) was added into each solution and allowed to dissolve for two days to elevate the saturation state of the fluid with respect to aragonite and promote crystallization. Fluids were filtered (0.7 μm particle retention) prior to the start of each experiment.

Aliquots of the solution (230 ml) were transferred to 300 ml Pyrex flasks connected to a 5 ml glass vial containing ammonium carbonate (Fig. 1). The parameters of the runs are listed in the Table 1. The temperature at which the aragonite precipitated was monitored through the course of the experiment using a mercury thermometer with subdivisions of 0.1 °C. A constant temperature of 22 ± 2 °C was achieved with air-conditioning in a closed room. A constant temperature of 53 ± 3 °C was achieved using a hot plate positioned beneath the flask. Thirteen days before the end of the experiments, we introduced a Dy spike into the solution of the run D-1 in order to provide a time marker that would be recorded in the Dy content of the crystal (34.33 mg of $DyCl_3 \cdot 6H_2O$ was added to the solution).

The duration of experiment conducted at 22 °C was 144 days (run D-1); the 53 °C experiment lasted for a total of 13 days (run D-2). Aragonite precipitated as needle-like crystals with a thickness of a few microns, radiating from a central point to form bundles of generally hemispherical shape. Hereafter these bundles are referred to as spherulites. Aragonite continuously nucleated at the surface of the solution and on the inner walls of the flask throughout each experiment (Fig. 1). The growth time of the particular spherulite of interest was estimated precisely (see Section 3 and Appendix 1). The diameter of the hemispherical bundles ranges from 300–900 μm. Sub-samples of both the solution and the crystals from run D-1 were taken four times during

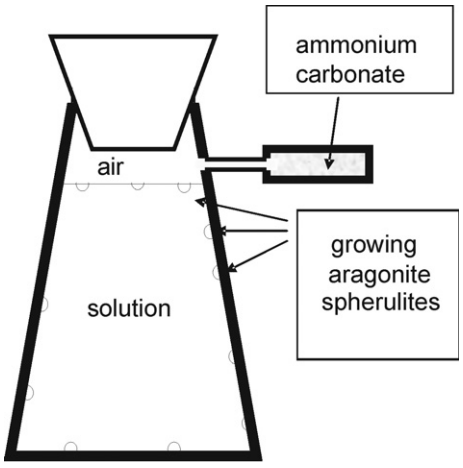

Fig. 1. Schematic diagram for the experimental apparatus used in the drift method. Hemispherical bundles of aragonite crystals grew in a Pyrex flask filled with chloride solution. See text for details.

Table 1
Analytical results of the initial, sub-sampled, and final experimental fluids

Probe no.	Run time (d)	t (d)	pH	DIC (mmol/kg)	CO_3^{2-} (mmol/kg)	Ca^{2+} (ppm)	Mg^{2+} (ppm)	U^{6+} (ppb)	Ω	log(R) (μmol/m^2 h)
D-1A	0	−116	6.75	0.17	3×10^{-4}	403 ± 3	1093 ± 8	6860 ± 8	6×10^{-3}	–
D-1B	73	−43	7.61	20.90	0.71	106 ± 2	1106 ± 9	2908 ± 7	3.3	1.9
D-1C (Dy)	131	15	7.98	53.92	3.80	24 ± 1	1107 ± 7	2723 ± 7	4.0	2.2
D-1D	144	28	7.65	64.32	1.95	23 ± 1	1102 ± 6	2681 ± 21	1.9	1.0
D-2[a]	13	N/A	7.81	N/A	N/A	39 ± 1	1064 ± 10	1445 ± 6	N/A	N/A

(Dy) = addition of dysprosium spike into solution; run time = time of each sub-sampling relative to the beginning of the run in days; t = growth time of the studied spherulite in days; DIC = dissolved inorganic carbon; Ca^{2+} and Mg^{2+} were measured by AA, U^{6+} by ICP-MS; Ω = saturation state; R = precipitation rate (see Appendix 2); N/A = none available; salinity (S) = 31.2; errors of 2σ are based on multiple replicate measurements, i.e., $2\sigma = SD/\sqrt{n}$.

Experiments were performed at 22 ± 2 °C, except run D-2 (53 ± 3 °C).

[a] In the run D-2 analyses were performed for the final fluids only.

the course of the experiment; each sampling involved 10 ml of solution and a few milligrams of crystals (Table 1). For run D-2, the solution was collected and crystals harvested only at the end of the run.

Hemispherical bundles of the crystals were removed from the flask using a metal spatula, rinsed with a calcite-saturated distilled water, dried under a heat lamp at 30–40 °C, and mounted in epoxy. The mounts were polished with fine Al_2O_3 powder (down to 0.3–1 μm size). An aliquot of each precipitate was analyzed by X-ray powder diffraction (XRD) to confirm that bulk material was aragonite. Analyses of a single spherulite with Renishaw M1000 micro-Raman spectrometer also yielded aragonite peak patterns. Center and the rim of the studied aragonite spherulite were examined with the spot of the size 5 and 2 μm, respectively. Microscope was depolarized.

Sub-samples of the experimental fluids were analyzed for dissolved inorganic carbon (DIC), Ca, Mg and U (Table 1). During the course of the experiments, the pH of the sub-sampled solutions was measured with an Orion gel-filled combination electrode (relative accuracy ±0.02) connected to an Orion meter (model 210A).

2.1. EMP and SIMS analyses

A JEOL 733 Superprobe wavelength-dispersive-electron-microprobe at Rensselaer Polytechnic Institute was used to analyze Ca, U, and Mg in the aragonite spherulites. We employed a 15 kV accelerating voltage and a 15–17 nA sample current with sample spot diameter of 20 μm and optimum counting time of 120 s. Standards of calcite (Ca = 40.04 wt%), uraninite (U = 79.34 wt%) and dolomite (Ca = 21.84 and Mg = 13.29 wt%) were used for Ca, U, and Mg analyses, respectively. SIMS measurements were conducted using a Cameca ims 3f ion microprobe at Woods Hole Oceanographic Institution employing a 4 nA primary O^- beam accelerated at 12.5 keV and a sample spot with a diameter of 10 μm. Following a 3 min pre-burn to remove the Au coat, a single spot was occupied while measuring secondary ion intensities for ^{163}Dy within a 30 eV window centered on an 80 eV offset from the peak of energy distribution. This energy filtering reduces molecular interferences to <0.1% (Hart and Cohen, 1996).

2.2. AA and ICP-MS analyses

Experimental solutions were analyzed for Ca with a Perkin–Elmer atomic absorption (AA) spectrometer (model 1100B) at Rensselaer Polytechnic Institute. A series of Ca and Mg standard solutions were prepared for machine calibration. A calcium stock solution of 1000 ppm (Fisher Scientific) was used for preparation of 1, 2.5, and 5 ppm of Ca in the 2% HNO_3. Magnesium standards of 0.1, 0.25, and 0.5 ppm were obtained by dilution of 1000 ppm stock (Fisher Scientific) solution. Analyses of ^{238}U were conducted using a Thermo-Finnigan Element2 inductively coupled plasma-mass spectrometer (ICP-MS) at Woods Hole Oceanographic Institution. Measurements were made at low resolution using indium as an internal standard at a concentration of 2.17 ppb in the 5% HNO_3. To calibrate the instrument, we prepared four U standard solutions of 0.86, 2.83, 4.40, and 6.85 ppb of U by dilution of 1000 ppm U stock solution (Alfa Aesar).

2.3. DIC analyses

Initial and final solutions and sub-samples from run D-1 were analyzed for dissolved inorganic carbon (DIC) by an automated system in which 0.3 ml samples were acidified with 2 ml of 1% H_3PO_4, and the evolved CO_2 stripped with N_2 gas and analyzed using a LICOR-6252 infrared analyzer at Woods Hole Oceanographic Institution (based on O'Sullivan and Millero, 1998). The instrument was calibrated using certified reference seawater samples supplied by A.G. Dickson (SIO). Precision was ±5 μmol/kg.

3. RESULTS

Spherulite interiors in experiments conducted at 22 °C are too dense to distinguish individual crystals, but tips of the radial crystals are visible at the rim (Fig. 2a). An example of a spherulite grown at 53 °C is shown in Fig. 2b. The less spherical shape and more easily distinguishable radial needles suggest that this spherulite grew more rapidly, forming a less dense structure than those precipitated at 22 °C. X-ray diffraction and micro-Raman spectroscopy confirmed that the precipitate is aragonite in all cases.

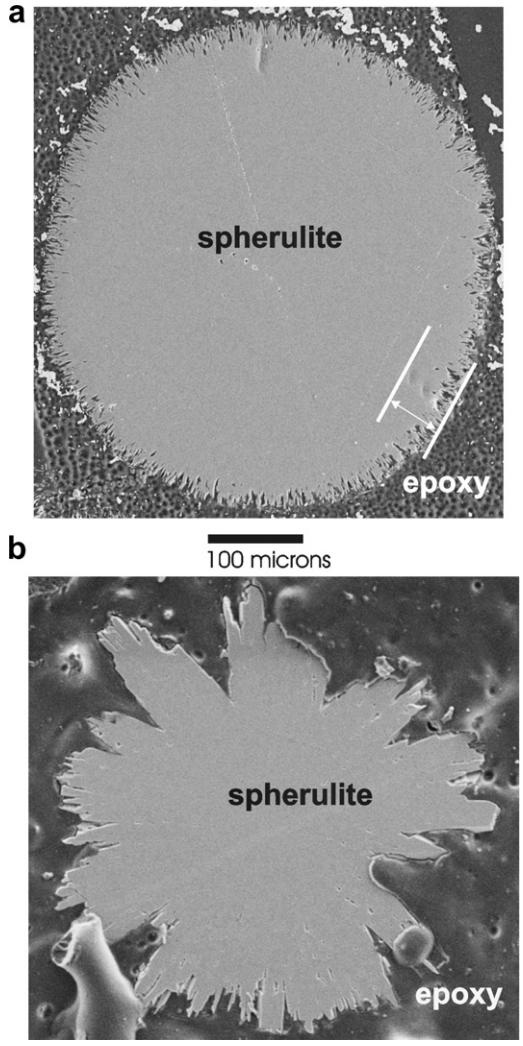

Fig. 2. An example of aragonite precipitates. Showed section is parallel to the aragonite-flask interface. (a) Spherulite with Dy spiked overgrowth from the run D-1 (22 °C). Spots correspond to the SIMS profiles from the edge to the center of the spherulite. Dy-spiked overgrowth is marked with lines and double-side arrow. (b) Spherulite grown at 53 °C.

3.1. Determination of growth rate

Growth rate of the aragonite spherulite was calculated using the width of the Dy spiked zone versus time elapsed between introduction of the spike and termination of the experiment. An estimate of growth rates in the interior of the spherulite was made assuming a cube root dependence of the spherulite radius on its volume with time (see Appendix 1). Bulk precipitation rate was calculated from the saturation state of the solution (Appendix 2).

For the Dy-based estimate, the width of the Dy-bearing overgrowth from aragonite spherulite (run D-1) was determined from the SIMS analytical profile that began at the edge of the spherulite and continued toward the center (Fig. 2a). This spherulite was analyzed for U/Ca and Mg/Ca as well. The Dy-spiked zone was found to have a width of 45 ± 10 μm (the error in these estimate correspond to analytical spot diameter of the Cameca ims 3f). Uncertainties in the growth rates were assigned on the basis of these uncertainties in overgrowth thickness. The average growth rate (V) was calculated from the width of the Dy-spiked layer and the duration of its growth (13 days) as $V = 45(\mu m)/13(d) = 3.5(\mu m/d) = 0.04(nm/s)$. This value can be considered the linear growth rate of individual needles or the radial growth rate of the host spherulite.

The radial growth rate was calculated at each point along a rim-core EMP profile made at a step interval of 30 μm:

$$V = dr/dt \quad (1)$$

where r and t are the spherulite radius and time of its growth, respectively. The relationship between r and t was determined from the inverse cube root dependence of r on the volume of the spherulite (see Fig. 3 and Appendix 1). Hence, the radial growth rate of the spherulite decreases with increasing time. Growth rate increases from 0.04 to 29.8 nm/s from the rim to the core of spherulite. The linear spherulite volume change should be proportional to the amount of Ca removed from the fluid. The above assumption is consistent with the linear fit of Ca concentration changes in the fluid between three data sub-sampled at 73, 131 and 144 days. The timing of the onset of spherulite

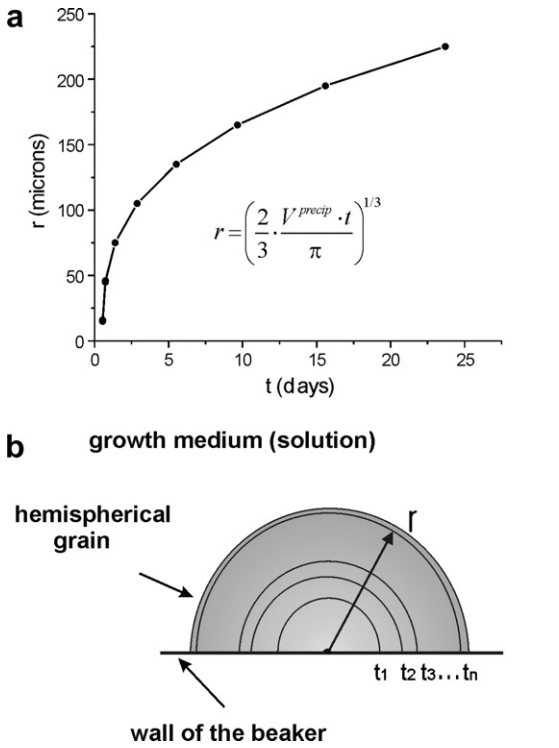

Fig. 3. Schematic diagram for determination of growth rate of the spherulites. At constant amount of aragonite precipitated per unit time, the cube of the radius varies linearly with time. The distance between zones (1, 2,...,n-1, n) is equal to 30 μm (the step of the EMP profiles), n is the number of the EMP measurements in the spherulite outward the center of crystallization at the crystal-flask interface.

crystallization ($t = 0$) was estimated at 116 days after beginning of the run D-1, hence $t = 28$ days at the end of experiment (144 days).

The estimation of bulk precipitation rates involved calculations based on the DIC and Ca analyses of the sub-sampled solutions in the run D-1 at 22 °C (see Appendix 2). Calculated precipitation rates are presented in the Table 1. The absence of a chemical marker (Dy) in aragonite and the lack of data on fluid composition of the experiment D-2 preclude constraint of aragonite growth history at 53 °C. Therefore V, change of fluid U/Ca and Mg/Ca, and hence K_d for U and Mg remained unknown at this temperature.

3.2. Composition of the aragonite spherulites

Electron microprobe profiles across the aragonite spherulites revealed that U/Ca and Mg/Ca ratios are highest in the core and decrease monotonically toward the rim in all cases (Fig. 4). Fig. 4a shows U/Ca ratios across four spherulites that had been sampled at different times through run D-1 (22 °C). The U/Ca ratios decrease from 3.04 to 0.67 mmol/mol from the core to the rim of the spherulites, with no significant differences observed amongst spherulites. In Fig. 4b, U/Ca profiles across two grains sampled from run D-2 (53 °C) are shown. The U/Ca ratios of aragonite grains precipitated at 53 °C are significantly higher than those grown at 22 °C, ranging from 5.51 mmol/mol at the center (compared with 3.04 at 22 °C) to 1.88 at the rim of the spherulite (compared with 0.67 at 22 °C). In Fig. 4c, Mg/Ca ratios generated across the same four spherulites as on the Fig. 4a. Here, the Mg/Ca ratios vary from 4.82 mmol/mol at the center and 0.63 at the edge of the spherulite. At 53 °C, there is a decrease in the ratios of Mg/Ca from 3.21 mmol/mol at the center (compared with 4.82 at 22 °C) to 0.71 at the edges of the spherulites (compared with 0.63 at 22 °C) (Fig. 4d).

Two out of 10 analyzed spherulites from run D-1, which was spiked with Dy 13 days before the end of the experiment, were found to have elevated Dy/Ca ratios near their rims. The SIMS profiles show a sharp increase of Dy/Ca ratio at a distance which is assumed to correspond to the time at which the Dy spike was introduced into solution. The large width of Dy-bearing overgrowth, which corresponds to ~2/3 of the total volume of the spherulite, combined with the small changes in fluid [Ca] sampled at 131 and 144 days (Table 1, D-1C and D-1D) suggest that growth of most spherulites stopped before or immediately after the Dy spike was introduced to the growth solution.

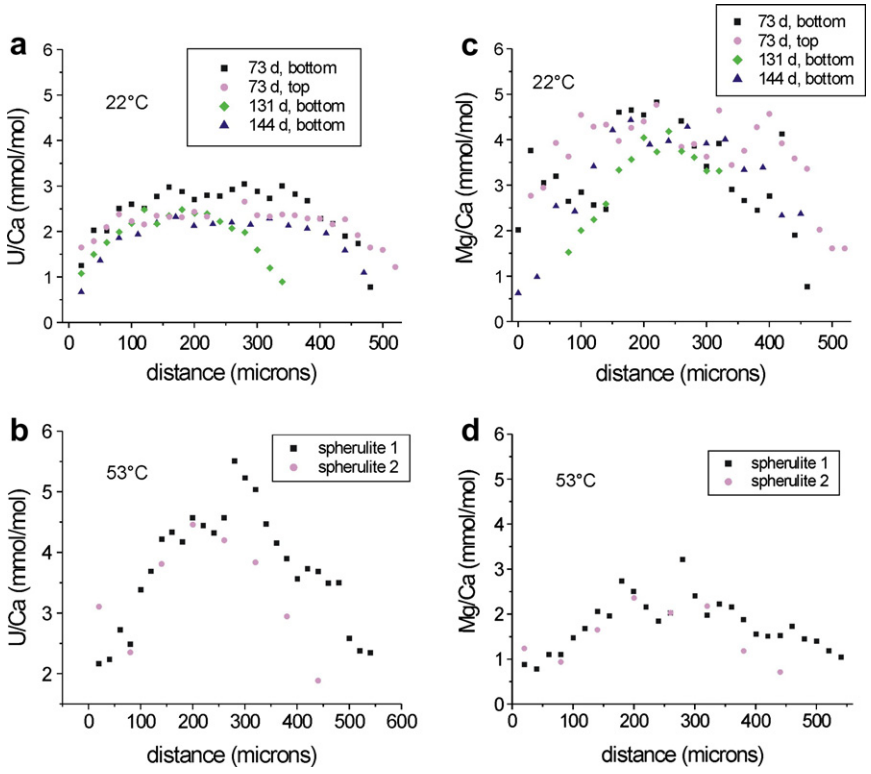

Fig. 4. The ratios of U/Ca and Mg/Ca across aragonite spherulites. Each rim to rim EMP profile started at distance of zero microns. d = days after beginning of the experiment; bottom = spherulites sampled from the bottom of the flask; top = spherulites sampled from the top of the flask (at the solution/air interface). (a) U/Ca ratios of the four aragonites from the run D-1 ($T = 22$ °C). Two spherulites were sub-sampled from the bottom and the top of the flask on the 73 day after beginning of the experiment. Another two spherulites were extracted from the bottom of the flask on the 131 and 144 day after beginning of the run. (b) U/Ca ratios of the two aragonites from the run D-2 ($T = 53$ °C). Spherulites were collected from the flask at the end of the experiment. (c and d) Runs D-1 ($T = 22$ °C) and D-2 ($T = 53$ °C), EMP profiles of Mg/Ca: description of spherulite locations are the same as for U/Ca plots.

3.3. Composition of the fluids

The concentration of Ca in the fluids, which is an indicator of the amount of aragonite that has precipitated, decreased with time during the experiments, as did the concentration of U. However, the U/Ca (mmol/mol) ratio of the aragonite was lower than that of the fluid, so the latter increased with time in run D-1 according to the relationship:

$$U/Ca = 0.223 \cdot t + 14.441, \quad R^2 = 0.97, \quad \text{for } -43 \leqslant t \leqslant 28 \tag{2}$$

where t is in days (Table 1, Fig. 5). In contrast, the concentration of Mg in the sub-sampled solutions remained uniform throughout the experiment due to its small partition coefficient (Table 1). However, since the Ca concentration of the fluid decreased, the Mg/Ca (mol/mol) ratio of fluid increased with time in run D-1 according to the equation:

$$Mg/Ca = 0.914 \cdot t + 57.385, \quad R^2 = 0.98, \quad \text{for } -43 \leqslant t \leqslant 28 \tag{3}$$

The pH value of the solution was in the range between 7.61 and 7.98 (see Table 1). Based on the calculations of Djogic et al. (1986) and Reeder et al. (2001)) the speciation of U^{6+} does not change significantly in the $CaCl_2$–NH_4Cl solution at pH range similar to this study. The dominant species in the pH range of this study is $UO_2(CO_3)_3^{4-}$.

In the run performed at 53 °C (D-2) only the final fluid was analyzed for Ca, Mg, and U (i.e., no sub-samples were taken). An initial solution was prepared with concentrations of Ca^{2+}, Mg^{2+}, and U^{6+} similar to those in run D-1 (Table 1). Both U/Ca and Mg/Ca ratios of the fluid increased over the course of experiment.

3.4. Partitioning of U and Mg between aragonite and fluid

The average partition coefficients of U (K_d^U) and Mg (K_d^{Mg}) in the Dy-spiked overgrowth layer of the spherulite

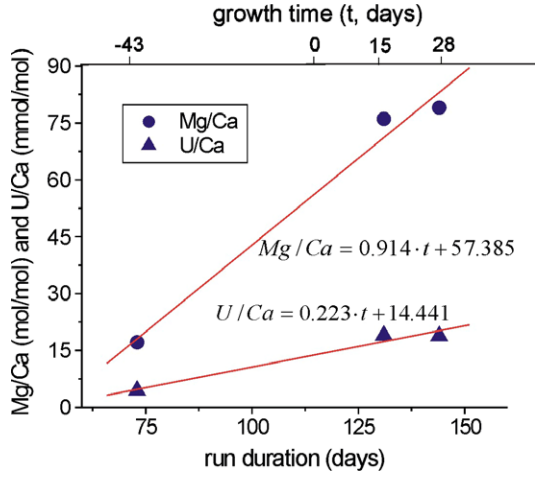

Fig. 5. Changes of the fluid U/Ca and Mg/Ca ratios with the time of the run D-1 at 22 °C. Here the lower x-axis represents the time from the beginning to the end of the run. The upper x-axis shows the time (t) of the crystallization of the studied spherulite.

were calculated using EMP data from this zone, together with the average ratios of the sub-sampled fluids C and D. The calculations yielded that $K_d^U = 0.046 \pm 0.011$ and $K_d^{Mg} = (1.90 \pm 1.27) \times 10^{-5}$ at $V = 0.040 \pm 0.014$ nm/s.

The trends of K_d^U and K_d^{Mg} versus V in the interior of the spherulite were calculated using U/Ca and Mg/Ca ratios in aragonite and fluid:

$$K_{dj}^i = \frac{(X_i/X_{Ca})_j^{\text{aragonite}}}{(X_i/X_{Ca})_j^{\text{fluid}}} \tag{4}$$

where X is the mole fraction of element i (U or Mg) and j is sample number (analysis spot and corresponding fluid sample; see Eqs. (2) and (3)). The mean values of U/Ca and Mg/Ca in the two core to rim profiles measured at similar distances from the center of the spherulite were used in the calculations of K_{dj}^U and K_{dj}^{Mg}, respectively; i.e., j varies from 1 to 7 (see Table 2). K_d^U and K_d^{Mg} increases rapidly as V increases from 0.04 to 0.2 nm/s, but the rate of increase slows when $V > 0.2$ nm/s (Figs. 6 and 7).

3.5. Modeling the experimental data using surface entrapment

The model of Watson and co-workers (Watson and Liang, 1995; Watson, 1996; Watson, 2004) was used to determine whether our experimental data are quantitatively consistent with the process of surface entrapment (see Appendix 3 for details of the calculations). According to this model, the near-surface region of a crystal is enriched (or possibly depleted) in the element of interest relative to the bulk lattice at thermodynamic equilibrium. If diffusion in the near-surface region is slow relative to the rate at which the interface advances into the growth medium, this chemically anomalous region is 'captured' by the crystal with varying degrees of efficiency. Given a constant temperature, the higher the growth rate, the greater the degree of entrapment. At very high growth rates, the lattice composition reflects that of the near surface region, representing maximum entrapment and the most extreme deviation possible from thermodynamic equilibrium. In our results, the plateaus of the K_d vs. V curves at high growth rates are believed to represent the case where surface entrapment has achieved 100% efficiency.

To apply the surface entrapment model to our results the concentration of Mg measured in our experimentally precipitated aragonite ($Mg_j^{\text{aragonite}}$) was compared to an estimate for the Mg concentration at thermodynamic equilibrium ($Mg_{eq}^{\text{aragonite}}$) (see Table 2 and Fig. 8). The value of $Mg_{eq}^{\text{aragonite}}$ was determined from the equilibrium Nernst partition coefficient by an approach similar to that of Gaetani and Cohen (2006) using the lattice strain theory of Blundy and Wood, 1994, 2003:

$$D_{Mg}^{\text{aragonite/fluid}} = \frac{Mg_{eq}^{\text{aragonite}}}{Mg^{\text{fluid}}} = D_{Ca}^{\text{aragonite/fluid}} \cdot \exp\left(-\frac{\Delta G_{\text{strain}}}{RT}\right) = 0.018 \text{ at } T = 22\ ^\circ\text{C} \tag{5}$$

where ΔG_{strain}, R and T are the strain energy, gas constant and temperature in Kelvin, respectively (for a detailed

Table 2
Data used for K_d calculations and modeling

V (nm/s)	$(U/Ca)^A$ (mmol/mol)	$(U/Ca)^F$ (mmol/mol)	$K_d^U \times 10^2$	Mg ($10^2 \times$ wt%)	$(Mg/Ca)^A$ (mmol/mol)	$(Mg/Ca)^F$ (mol/mol)	$K_d^{Mg} \times 10^5$
0.040 ± 0.014	0.88 ± 0.24	19.725	4.48 ± 1.26	3.6 ± 1.1	1.50 ± 1.01	79.041	1.90 ± 1.27
0.059 ± 0.019	1.47 ± 0.21	17.919	8.23 ± 1.30	4.0 ± 1.1	1.66 ± 0.99	71.642	2.31 ± 1.38
0.084 ± 0.028	1.91 ± 0.25	16.593	11.51 ± 01.71	7.1 ± 1.1	2.96 ± 0.95	66.206	4.48 ± 1.44
0.132 ± 0.044	2.00 ± 0.25	15.672	12.76 ± 1.87	6.9 ± 1.1	2.88 ± 0.95	62.432	4.62 ± 1.53
0.234 ± 0.078	2.16 ± 0.25	15.083	14.32 ± 2.04	8.9 ± 1.1	3.71 ± 0.97	60.017	6.18 ± 1.62
0.520 ± 0.174	2.31 ± 0.26	14.751	15.63 ± 2.17	9.8 ± 1.1	4.06 ± 0.98	58.655	6.93 ± 1.67
1.944 ± 0.666	2.14 ± 0.26	14.604	14.65 ± 2.15	10.5 ± 1.1	4.36 ± 1.01	58.053	7.51 ± 1.74
29.82 ± 22.23	2.18 ± 0.26	14.564	14.97 ± 2.17	9.5 ± 2.4	3.93 ± 0.99	57.888	6.79 ± 1.71

Superscripts A and F indicates the elemental ratios in aragonite and fluid, respectively; Mg is from EMP analyses; errors for $(U/Ca)^A$, $(Mg/Ca)^A$, and Mg are 2σ of EMP measurements; errors for the fluid ratios are the standard deviations from the linear fits divided by the square root of the numbers of data points (Eqs. (2) and (3)), i.e., ± 1.22 mmol/mol for $(U/Ca)^F$ and ± 3.70 mol/mol for $(Mg/Ca)^F$.

description of the calculations see Gaetani and Cohen (2006)).

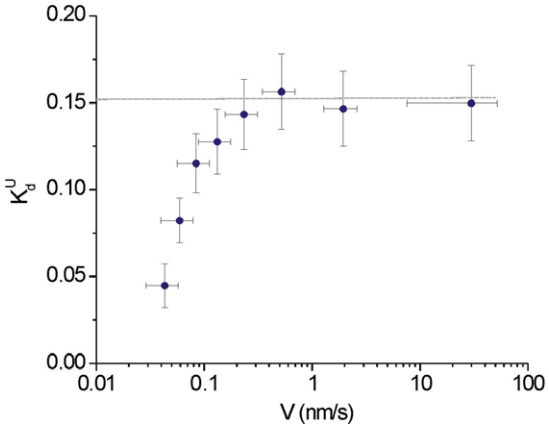

Fig. 6. Partitioning of U into aragonite versus growth rate at 22 °C (run D-1). Spherulite was collected at the end of the run, i.e., 144 days from the beginning of experiments. The growth time of spherulite was estimated as 28 days. Dashed line corresponds to the maximum K_d^U value. Errors are 2σ.

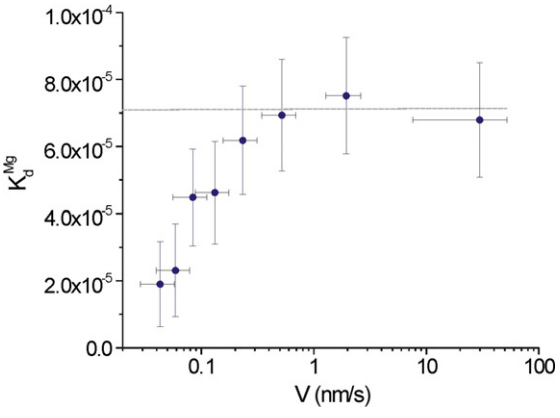

Fig. 7. Partitioning of Mg into aragonite versus growth rate at 22 °C (run D-1). See Fig. 6 for description.

Fig. 8 is a comparison of the relationship between $Mg_j^{aragonite}/Mg_{eq}^{aragonite}$ and V determined in our experiments (triangles) and predicted by surface entrapment (circles). These results show that $Mg_j^{aragonite}/Mg_{eq}^{aragonite}$ becomes independent of growth rate at $V \geqslant 2$ nm/s (or 173 μm/day), suggesting perfect (100%) 'capture' of the surface composition during growth at these high rates. Equilibrium aragonite (i.e., no surface entrapment) requires $V < 10^{-3}$ nm/s (or 0.09 μm/day). The surface entrapment model was not explored in detail with our U data because this element is incorporated into aragonite as $UO_2(CO_3)_3^{4-}$ (Reeder et al., 2000), essentially precluding estimation of equilibrium partitioning using the lattice-strain approach.

4. DISCUSSION

Our data show that U and Mg partitioning into abiogenic aragonite is strongly influenced by crystal growth rate. As demonstrated above, the observed trends—sharp increases in K_d^U and K_d^{Mg} at low growth rates and plateaus at high growth rates—are quantitatively consistent with predictions of the growth entrapment model of Watson and co-workers (Watson and Liang, 1995; Watson, 1996; Watson, 2004). That K_d^U and K_d^{Mg} increase with increasing linear growth rate indicates that Mg and U are both enriched in the near surface region of aragonite relative to the bulk lattice. While development of a depleted fluid boundary layer adjacent to the growing crystal is also capable of producing growth rate-dependent partitioning, calculations carried out using Eq. 10 of Smith et al. (1955) and cation diffusivities compiled by Li and Gregory (1974) indicate that this effect is minimal at the linear growth rates in our experiments.

Our results have implications for interpreting the Mg/Ca and U/Ca ratios of biogenic aragonites, where a dependence of the element:calcium ratio upon crystal growth rate can be expected even under isothermal conditions. The dependence of U/Ca and Mg/Ca ratios on crystal growth rate should be evident in the growth rate range of $0.040 \leqslant V \leqslant 0.2$ nm/s i.e., 3.5–17 μm/day, which is well within the range exhibited by corals. Extremely low growth rates ($V < 10^{-3}$ nm/s or 0.09 μm/day in case of Mg) would result in no entrapment at all, and the composition of the

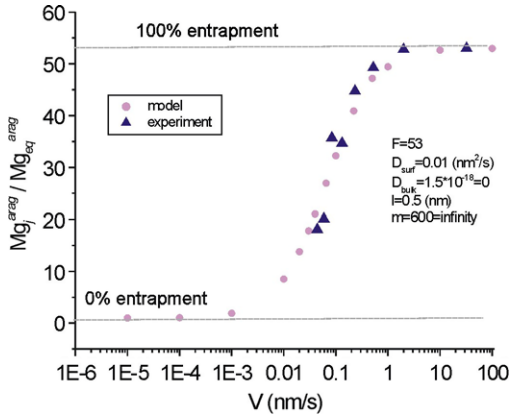

Fig. 8. Ratio of measured Mg to its equilibrium value versus aragonite growth rate. Triangles and circles represent experimental and calculating data, respectively. Upper dashed line shows the highest degree of entrapment when lattice composition approaching those of surface. Lower dashed line corresponds to the equilibrium growth without surface entrapment.

crystal would represent true thermodynamic equilibrium (Fig. 8).

While K_d^U and K_d^{Mg} both increase with increasing V at 22 °C, they exhibit opposite dependencies upon temperature between 22 and 53 °C. In runs D-1 and D-2, the differences in fluid composition (U/Ca and Mg/Ca) at these two temperatures cannot explain the inverse variation of U/Ca and Mg/Ca in the experimental aragonite. We believe, therefore, that this variation reflects the effect of temperature on the partitioning of Mg and probably U between the fluid and the near-surface region of the aragonite. The similar shapes element:calcium profiles in the low and high temperature runs suggest that the value of the near surface diffusivity at 53 °C is insufficient to preclude the surface entrapment of Mg and U. The decrease of Mg/Ca ratios with increasing temperature is consistent with results of Gaetani and Cohen (2006). The observed diminution of Mg/Ca and increase in U/Ca with increasing temperature is opposite to the trends observed in coral skeletons, where Mg/Ca ratios show a positive dependence on temperature (Wei et al., 2000; Watanabe et al., 2001) and U/Ca ratios are negatively correlated with temperature (e.g., Min et al., 1995). This suggests that temperature is not the dominant control on Mg/Ca and probably U/Ca ratios in coral aragonite. Further, our results indicate that variations in crystal growth rate can not explain the inverse correlation between U/Ca and Mg/Ca observed in both cold and warm-water corals (Sinclair et al., 2006). If crystal growth rate were the dominant influence on compositional variability in this coral, our results suggest that Mg/Ca and U/Ca should be positively, not negatively, correlated. Several studies have shown that variations in the Mg/Ca ratios of coral skeleton are consistent with Rayleigh fractionation (Cohen et al., 2006; Gaetani and Cohen, 2006; Gagnon et al., 2007). This may also be the case for U although, as discussed below, variations in pH of the calcifying fluid may also be important.

We compared our data with previous studies in which bulk precipitation rates rather than crystal growth rates were determined by estimating the precipitation rates of our experimental aragonites using the empirical equation of Zhong and Mucci (1989) (see Appendix 2). The estimated range of aragonite precipitation rates was 1.0–2.2 μmol m^{-2} h^{-1} (Table 1). It is possible that precipitation rate obtained by the saturation state method may not be entirely appropriate for our experiments because the dissociation constants K_1 and K_2 are for seawater, and we used $NaCl(NH_4Cl)$–$MgCl_2$–$CaCl_2$ solutions in this study. Nevertheless, we made a first order comparison (Fig. 9) of our data against those generated by Zhong and Mucci (1989) and Gaetani and Cohen (2006). Our datum represents the K_d^{Mg} determined in Dy-spiked layer, where the precipitation rate was obtained from the fluid sub-sample D1-C (Table 1). The difference from other experimental results may lie in the difference in experimental design and analytical techniques. Gaetani and Cohen (2006) analyzed Mg/Ca ratios in the centers of the spherulites using SIMS ion probe. In contrast, Zhong and Mucci (1989) analyzed Mg/Ca ratio of the bulk precipitate that may have contained some calcite. In addition, in this work as well as in Gaetani and Cohen (2006) the authors did not use seed material in the experimental setup as was done by Zhong and Mucci (1989). Therefore, in the present work and that of Gaetani and Cohen (2006), the aragonite surface area was a strong function of time, in contrast to the case in the study of Zhong and Mucci (1989).

Our $K_d^U - V$ relationship is opposite to that observed by Meece and Benninger (1993). They showed that U partitioning between aragonite and seawater decreases with increasing precipitation rate and increasing pH of solution. The difference in pH between our experiments (pH = 7.61–7.98) and theirs (8.0–8.8) may explain these opposite $K_d^U - V$ trends. Calculations of U speciation in seawater from Djogic et al. (1986) showed that over the pH range of fluid from our experiment the mole fraction of $UO_2(CO_3)_3^{4-}$ does not change significantly, and is equal

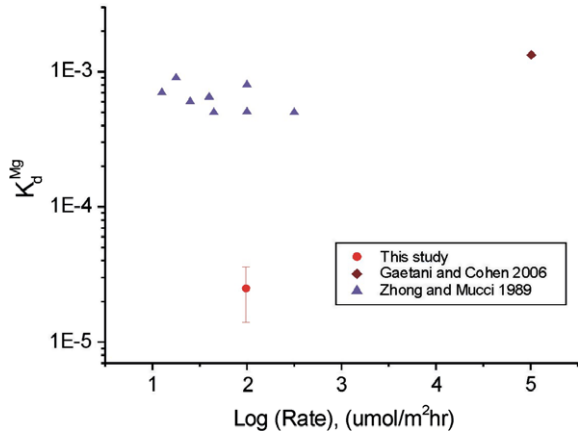

Fig. 9. Comparison of Mg partitioning data from this study with previous ones. Triangles – Zhong and Mucci (1989); diamond – Gaetani and Cohen, 2006); circle – this study. Bulk precipitation rate (μmol/m^2h) was calculated from the value of Ω of the fluid subsampled just before addition of the Dy spike (at 131 days after beginning of the run) using Eq. A2.5 (see Appendix 2).

to ~0.9. With increasing of pH between the runs of Meece and Benninger (1993) the mole fraction of $UO_2(CO_3)_3^{4-}$ decrease from ~0.9 down to ~0.7 and mole fraction of $UO_2(OH)_3^-$ increased from ~0.1 to ~0.3 (see Djogic et al., 1986; Fig. 1a and b). Reeder et al., 2000) showed that U is incorporated into aragonite in the form of its aqueous species $UO_2(CO_3)_3^{4-}$. Therefore it is likely that increase of pH from 8.0 to 8.8 causes a decrease in the mole fraction of $UO_2(CO_3)_3^{4-}$, lowering the partition coefficient of U in the experiments of Meece and Benninger (1993). This interpretation suggests that the changes in U uptake they observed might have been due to differences in U speciation rather than changes in precipitation rate.

5. CONCLUSIONS

Partitioning of Mg and U between aragonite and fluid both exhibits a strong positive dependence on growth rate in a manner that is consistent with the growth entrapment model. According to the model magnesium and probably uranium are enriched in the aragonite near-surface region relative to the bulk lattice. The changes of K_d^{Mg} with aragonite growth rate were described by surface entrapment model quantitatively. The degree of Mg incorporation into aragonite decreases with increasing temperature from 22 to 53 °C.

ACKNOWLEDGEMENT

We would like to thank Jerzy Blusztajn, Dave Schneider, and William Martin for helping to perform ICP-MS and gas chromatography analyses; Daniel McCorkle for fruitful discussion about calculation of the fluid saturation states. We also thank Nobumichi Shimizu and Graham Layne, for helping with SIMS 3f analyses; George Rossman and Benjamin Harrison for helping to perform micro-Raman spectroscopy and XRD analyses. We thank Miryam Bar-Matthews, Patricia Dove, Laura Wasylenki, Daniel Sinclair, and three anonymous reviewers for their helpful review of the previous version of the manuscript. This work was supported by the National Science Foundation (NSF) through grant no. EAR-0337481 to E.B. Watson. SIMS analyses were covered by NSF through grant nos. OCE-0347328, OCE-0402728, and OCE-0527350 to G.A. Gaetani and A.L. Cohen.

APPENDIX 1. ESTIMATIONS OF THE GROWTH RATE (V) CHANGES THROUGH THE WHOLE SPHERULITE

Volume change of the analyzed spherulite was determined from its hemispherical geometry with radius r.

$$\text{Volume} = \frac{2}{3}\cdot\pi r^3 \tag{A1.1}$$

Volumes of the growing spherulite were calculated at time (τ) when Dy-spike was added ($\tau = 131$ days, $r = 195$ μm, volume = 15531805 μm^3) and at the end of the experiment ($\tau = 144$ days, $r = 240$ μm, volume = 28938240 μm^3). The linear behavior of volume(τ) at $73 \leqslant \tau \leqslant 144$ was assumed and fitting of two above (τ; volume) data-points yielded:

$$\text{Volume}(\tau) = 1032033\cdot\tau + 119674578 \tag{A1.2}$$

Extrapolation of volume to the earlier times showed its approaching 0 at 116 days after beginning of the run, i.e., spherulite growth time (t) was set to 0 ($t = 0$ when $\tau = 116$ days). The spherulite volume change with growth time can be described as:

$$\text{Volume}(t) = 1032033\cdot t + 1054 \tag{A1.3}$$

The spherulite volume was calculated for each r values (the distance of EMP analytical spots from the center of the spherulite). Then τ and t were calculated for each analyzed spot using Eqs. (A1.2) and (A1.3). The growth rate values (V) were calculated for each distance between the EMP spots:

$$\Delta V_n = \Delta r/\Delta t \tag{A1.4}$$

where $\Delta r = 30$ μm is the distance between EMP spots, Δt is the calculated time interval required for growth of each layer with the thickness Δr, and n is the number of the analyzed spot.

APPENDIX 2. ESTIMATION OF ARAGONITE BULK PRECIPITATION RATES FROM FLUID COMPOSITION

The values of $[CO_3]^{2-}$ were calculated using equation from Zeebe and Wolf-Gladrow, 2001) p. 4:

$$[CO_3^{2-}] = \frac{DIC}{1 + \frac{10^{-pH}}{K_2} + \frac{10^{-2pH}}{K_1K_2}} \tag{A2.1}$$

where K_1 and K_2 are the constants of the dissociation of carbonic acid in the seawater:

$$CO_2 + H_2O = HCO_3^- + H^+ \ (K_1)$$
$$HCO_3^- = CO_3^{2-} + H^+ \ (K_2)$$

The dissociation constants were calculated using interpolating equations for the combined data of Hansson (1972) and Mehrbach et al. (1973) presented in Dickson and Millero (1987) for 25 °C and salinity (S) of 31.1:

$$pK_1 = \frac{845}{T(K)} + 3.284 - 0.0098\cdot S + 8.7\cdot 10^{-5}\cdot S^2 = 5.936 \tag{A2.2}$$

$$pK_2 = \frac{1377.3}{T(K)} + 4.824 - 0.0185\cdot S + 1.22\cdot 10^{-4}\cdot S^2 = 9.048 \tag{A2.3}$$

The saturation state (Ω) of the fluid was calculated using the following equation:

$$\Omega = \frac{[Ca]^{2+}\cdot[CO_3]^{2-}}{K^*_{sp}} \tag{A2.4}$$

The solubility product of aragonite (K^*_{sp}) was calculated using the expression developed by Mucci (1983), yielding $pK^*_{sp} = 6.24$. The bulk precipitation rate (R in $\mu mol\cdot m^{-2}\cdot h^{-1}$) of aragonite from seawater of 3.5% salinity at 25°C was calculated using the equation of Zhong and Mucci (1989):

$$\log(R) = 2.36\cdot\log(\Omega - 1) + 1.09 \tag{A2.5}$$

APPENDIX 3. PARAMETERS FOR SURFACE ENTRAPMENT MODEL

The calculations were processed using the equation proposed by Watson (2004):

$$\mathrm{Mg}(x) = \mathrm{Mg}_{eq} \cdot F^{\exp(x/l)} \quad \text{(A3.1)}$$

where $Mg(x)$ is the concentration of Mg in the crystal at some distance x from the surface, Mg_{eq} is the concentration reflecting partition equilibrium between the growth medium and the bulk crystal, F is the surface enrichment factor and l is the half-thickness of the enriched surface layer.

In order to match the experimental data the values of F and l were set as 53 and 0.5 nm, respectively. The enrichment factor (F) was taken as the ratio of maximum measured Mg concentration to the equilibrium value ($\mathrm{Mg}_{\mathrm{eq}}^{\mathrm{aragonite}}$). The lattice diffusivity was considered as ~0, because it is negligibly small at ambient temperatures. Therefore, the only diffusivity that affects the crystal composition is D_{surf} (the diffusivity in the chemically distinct, near-surface layer).

The parameters of D_{surf} and m were optimized for obtaining the best fit of experimental data. The best fit was achieved when the Mg diffusion coefficient in the chemically distinct, near-surface layer (D_{surf}) and the distance multiplier (m) were set to 0.01 nm^2/s and infinity (∞), respectively. The meaning of infinite m is that the diffusivity is independent of depth in the crystal (and equal to D_{surf}) over a distance much greater than the thickness of the compositionally distinct near-surface layer.

REFERENCES

Blundy J. and Wood B. (1994) Prediction of crystal-melt partition coefficients from elastic moduli. *Nature* **372**, 452–454.

Blundy J. D. and Wood B. J. (2003) Partitioning of trace elements between crystal and melt. *Earth Planet. Sci. Lett.* **372**, 452–454.

Cardinal D., Hamelin B., Bard E. and Pätzold J. (2001) Sr/Ca, U/Ca, and $\delta^{18}O$ records in recent massive corals from Bermuda: relationships with sea surface temperature. *Chem. Geol.* **176**, 213–233.

Cohen A. L., Layne G. D., Hart S. R. and Lobel P. S. (2001) Kinetic control of skeletal Sr/Ca in a symbiotic coral: implications for the paleotemperature proxy. *Paleoceanography* **16**, 20–26.

Cohen A. L., Gaetani G. A., Lundälv T., Corliss B. H. and George R. Y. (2006) Compositional variability in the cold-water scleractinian, *Lophelia pertusa*: new insight into "vital effects. *Geochem. Geophys. Geosys.* **7**, 12004. doi:10.1029/2006GC001354.

Cohen A. L. and Thorrold S. R. (2007) Recovery of temperature records from slow-growing corals by fine scale sampling of skeletons. *Geophys. Res. Lett.* **34**, L17706. doi:10.1029/2007GL030967.

Djogic R., Sipos L. and Branica M. (1986) Characterization of uranium (VI) in seawater. *Limnol. Oceanogr.* **31**, 1122–1131.

Dickson A. G. and Millero F. G. (1987) A comparison of equilibrium constants for the dissociation of carbonic acid in seawater media. *Deep-Sea Res. A-Oceanogr. Res. Papers* **34**, 1733–1743.

Gabitov R. I. and Watson E. B. (2006) Partitioning of strontium between calcite and fluid. *Geochem. Geophys. Geosys.* **7**, Q11004. doi:10.1029/2005GC001216.

Gaetani G. A. and Cohen A. L. (2006) Element partitioning during precipitation of aragonite from seawater: a framework for understanding paleoproxies. *Geochim. Cosmochim. Acta* **70**, 4617–4634.

Gagnon A. C., Adkins J. F., Fernandez D. P. and Robinson L. F. (2007) Sr/Ca and Mg/Ca vital effects correlated with skeletal architecture in a scleractinian deep-sea coral and the role of Rayleigh fractionation. *Earth Planet. Sci. Lett.* **261**, 280–295.

Gruzensky P. M. (1967) Growth of calcite crystals. *J. Phys. Chem. Solids S* **1**, 365–367.

Hansson I. (1972) An analytical approach to the carbonate system in seawater. Ph.D. Thesis, University of Goteborg, Sweden.

Hart S. R. and Cohen A. L. (1996) An ion probe study of annual cycles of Sr/Ca and other trace elements in corals. *Geochim. Cosmochim. Acta* **60**, 3075–3084.

Kinsman D. J. J. and Holland H. D. (1969) The co-precipitation of cations with $CaCO_3$-IV. The co-precipitation of Sr^{2+} with aragonite between 16 and 96 °C. *Geochim. Cosmochim. Acta* **33**, 1–17.

Kitano Y. and Oomori T. (1971) The coprecipitation of uranium with calcium carbonate. *J. Oceanogr. Soc. Japan* **27**, 34–42.

Li Y.-H. and Gregory S. (1974) Diffusion of ions in sea water and in deep-sea sediments. *Geochim. Cosmochim. Acta* **38**, 703–714.

Lorens R. B. (1981) Sr, Cd, Mn, and Co distribution coefficients in calcite as a function of calcite precipitation rate. *Geochim. Cosmochim. Acta* **45**, 553–561.

Meece D. E. and Benninger L. K. (1993) The coprecipitation of Pu and other radionuclides with $CaCO_3$. *Geochim. Cosmochim. Acta* **57**, 1447–1458.

Mehrbach C., Culberson C. H., Hawley J. E. and Pytkowicz R. M. (1973) Measurement of the apparent dissociation constants of carbonic acid in seawater at atmospheric pressure. *Limnol. Oceanogr.* **18**, 897–907.

Meibom A., Cuif J.-P., Hillion F., Constantz B. R., Juillet-Leclerc A., Dauphin Y., Watanabe T. and Dunbar R. B. (2004) Distribution of magnesium in coral skeleton. *Geophys. Res. Lett.* **31**, L23306. doi:10.1029/2004GL021313.

Meibom A., Yurimoto H., Cuif J-P., Domart-Coulon I., Houlbreque F., Constantz B., Dauphin Y., Tambutte E., Tambutte S., Allemand D., Wooden J. and Dunbar R. (2006) Vital effects in coral skeletal composition display strict three-dimensional control. *Geophys. Res. Lett.* **33**, L11608. doi:10.1029/2006GL025968.

Min G. R., Edwards R. L., Taylor F. W., Recy J., Gallup C. D. and Beck J. W. (1995) Annual cycles of U/Ca in coral skeletons and U/Ca thermometry. *Geochim. Cosmochim. Acta* **59**, 2025–2042.

Mitsuguchi T., Matsumoto E., Abe O., Uchida T. and Isdale P. J. (1996) Mg/Ca thermometry in coral skeletons. *Science* **274**(5289), 961–963.

Mucci A. (1983) The solubility of calcite and aragonite in seawater at various salinities, temperatures, and one atmosphere total pressure. *Am. J. Sci.* **283**, 780–799.

O'Sullivan D. W. and Millero F. J. (1998) Continual measurement of the total inorganic carbon in surface seawater. *Mar. Chem.* **60**, 75–83.

Quinn T. M. and Sampson D. E. (2002) A multiproxy approach to reconstructing sea surface conditions using coral skeleton geochemistry. *Paleoceanography* **17**, 1062. doi:10.1029/2000PA000528.

Reeder R. J., Nugent M., Lamble G. M., Tait C. D. and Morris D. E. (2000) Uranyl incorporation into calcite and aragonite: XAFS and luminescence studies. *Environ. Sci. Technol.* **34**, 638–644.

Reeder R. J., Nugent M., Tait C. D., Morris D. E., Heald S. M., Beck K. M., Hess W. P. and Lanzirotti A. (2001) Coprecip-

itation of uranium (VI) with calcite: XAFS, micro-XAS, and luminescence characterization. *Geochim. Cosmochim. Acta* **65**, 3491–3503.

Reynaud S., Ferrier-Page C., Meibom A., Mostefaoui S., Mortlock R., Fairbanks R. and Allemand D. (2007) Light and temperature effects on Sr/Ca and Mg/Ca ratios in the scleractinian coral Acropora sp. *Geochim. Cosmochim. Acta* **71**, 354–362.

Robinson L. F., Adkins J. F., Fernandez D. P., Burnett D. S., Wang S.-L., Gagnon A. C. and Krakauer N. (2006) Primary U distribution in scleractinian corals and its implications for U series dating. *Geochem. Geoph. Geosys.* **7**, Q05022. doi:10.1029/2005GC001138.

Shen G. T. and Dunbar R. B. (1994) U/Ca in reef corals – another ocean thermometer? *Eos Trans.*, AGU 75, O21L-1, p. 79.

Sinclair D. J., Kinsley L. P. J. and McCulloch M. T. (1998) High resolution analysis of trace elements in corals by laser ablation ICP-MS. *Geochim. Cosmochim. Acta* **62**, 1889–1901.

Sinclair D. J., Williams B. and Risk M. (2006) A biological origin for climate signal in corals – the trace elements "vital effects" and ubiquitous in scleractinian coral skeletons. *Geophys. Res. Lett.* **33**, L17707. doi:10.1029/2006GL027183.

Smith V. G., Tiller W. A. and Rutter J. W. (1955) A mathematical analysis of solute redistribution during solidification. *Can. J. Phys.* **33**, 723–745.

Tesoriero A. J. and Pankow J. F. (1996) Solid solution partition of Sr^{2+}, Ba^{2+}, and Cd^{2+} to calcite. *Geochim. Cosmochim. Acta* **60**, 1053–1063.

Watanabe T., Winter A. and Oba T. (2001) Seasonal changes in sea surface temperature and salinity during the Little Ice Age in the Caribbean sea deduced from Mg/Ca and $^{18}O/^{16}O$ ratios in corals. *Mar. Geol.* **173**, 21–35.

Watson E. B. and Liang Y. (1995) A simple model for sector zoning in slowly growing crystals: implications for growth rate and lattice diffusion, with emphasis on accessory minerals in crustal rocks. *Am. Mineral.* **80**, 1179–1187.

Watson E. B. (1996) Surface enrichment and trace-element uptake during crystal growth. *Geochim. Geochim. Cosmochim. Acta* **60**, 5013–5020.

Watson E. B. (2004) A conceptual model for near-surface kinetic controls on the trace-element and stable isotope composition of abiogenic calcite crystals. *Geochim. Cosmochim. Acta* **68**, 1473–1488.

Wei G., Sun M., Li X. and Nie B. (2000) Mg/Ca, Sr/Ca, and U/Ca ratios of a porites coral from Sanya Bay, Hainan Island, South China Sea and their relationships to sea surface temperature. *Palaeogeogr. Palaeoclimatol. Palaeoecol.* **162**, 59–74.

Zeebe R. E. and Wolf-Gladrow D. (2001) CO_2 in seawater: equilibrium, kinetics, isotopes. *Elsevier Oceanogr. Ser.* **65**, 346.

Zhong S. and Mucci A. (1989) Cacite and aragonite precipitation from seawater of various salinities: precipitation rates and overgrowth compositions. *Chem. Geol.* **78**, 283–299.

Associate editor: Miryam Bar-Matthews